Z. Phys. D 35, 285–297 (1995)

ZEITSCHRIFT
FÜR PHYSIK D

Electron-gas clusters: the ultimate jellium model

M. Koskinen[1,*], P.O. Lipas[1], M. Manninen[2,]**

[1] Department of Physics, University of Jyväskylä, P.O. Box 35, FIN-40351 Jyväskylä, Finland
[2] Niels Bohr Institute, Blegdamsvej 17, DK-2100 Copenhagen Ø, Denmark

Received: 5 May 1995

Abstract. The local spin-density approximation is used to calculate ground- and isomeric-state geometries of jellium clusters with 2 to 22 electrons. The positive background charge of the model is completely deformable, both in shape and in density. The model has no input parameters. The resulting shapes of the clusters exhibit breaking of axial and inversion symmetries; in general the shapes are far from ellipsoidal. Those clusters which lack inversion symmetry are extremely soft against odd-multipole deformations. Some clusters can be interpreted as molecules built from magic clusters. The deformation produces a gap at the Fermi level. This results in a regular odd-even staggering of the total energy per electron and of the HOMO level. The strongly deformed 14-electron cluster is semimagic. Stable isomers are predicted. The splitting of the plasmon resonance due to deformation is estimated on a classical argument.

PACS: 36.40.+d; 73.20.Mf; 73.20.Dx; 21.60.Cs

1 Introduction

Following the observation of electronic magic numbers by Knight et al. [1] many properties of alkali-metal clusters have been explained with the simple jellium model, where the interacting valence electrons move in the Coulomb potential of a homogeneous background charge [2]. The magic numbers can be explained with a spherical jellium model [3–5]. However, for understanding the odd-even staggering of the binding energy per electron [2, 6–8] and the splitting of the plasmon resonance [9, 10], one has to use a spheroidal [11] or triaxial [12] model. The jellium model can be further improved by taking into account higher multipole deformations [13] and allowing a finite thickness for the surface of the background charge [14, 15]. Furthermore, several models have been suggested for including the effect of discrete ions [16–20] in the jellium model.

In the present paper we study the properties of a jellium model where the background density is completely deformable. This leads to the result that the background density is everywhere equal to the valence-electron density, so that there will be no net charge density or corresponding Coulomb energy. The effective potential which holds the cluster together is the exchange-correlation potential. We calculate the cluster geometries by using the local-spin-density approximation (LSDA) in a plane-wave basis. No symmetry restrictions are imposed on the electron density.

The study of such a simple model is motivated by the following considerations:

(1) There are no free parameters in the model. The bulk limit of the model is a homogeneous electron gas with a density which minimizes the total energy per electron ($r_s = 4.18a_0$). In the present model, there will be no artificial effects due to a tendency of the electron gas towards this density. In the conventional jellium model, the tendency towards equilibrium density leads to negative surface energies in the case of high-density metals.
(2) The total energy of a jellium cluster can be lowered by allowing more and more freedom to relax the background charge, both its shape and its density profile. The present model constitutes the ultimate limit of this relaxation process: varying the background charge can no longer reduce the total energy.
(3) The model represents the shapes and densities favored by the valence electrons. In real metal clusters, the shapes will be determined by the interplay between the electrons and the discrete ions. Our model determines the optimal shapes from the electrons' point of view.
(4) Since we include the spin dependence of the exchange-correlation energy, we can study the effect of exchange splitting on the odd-even staggering.

**Present address:* NORDITA, Blegdamsvej 17, DK-2100 Copenhagen Ø, Denmark
***Permanent address:* Department of Physics, University of Jyväskylä, FIN-40351 Jyväskylä, Finland

(5) The local-density description of an electron-hole plasma in semiconductors [21] is closely related to our model. More specifically, our model can describe excitonic electron-hole clusters. The same effective mass is then assumed for particles and holes, and no electron-hole correlation is taken into account.
(6) Since our model describes fermions bound by a density-dependent potential, it is applicable to other fermion clusters, namely, nuclei and clusters of ^{3}He.

Since the bulk density in our model is close to that of sodium or potassium, we can compare our results with experiments on these metals. Nevertheless, our aim is to obtain a further understanding of the basic trends and to make only qualitative comparisons with experimental results. There exist a great many detailed electronic-structure calculations which use realistic pseudopotentials and a configuration-interaction (CI) or local-density-approximation (LDA) description of the electronic Hamiltonian [22–25]. These methods, however, are applicable only to the smallest clusters; for them, they are superior to ours in making quantitative comparisons between theory and experiment.

The plan of the paper is as follows. In Sect. 2 we describe the ultimate jellium model. We describe in some detail the numerical computations and the methods used in analyzing the electron densities. The results for clusters with 2 to 22 electrons are given in Sect. 3: ground-state properties in Subsects. 3.1 to 3.4, isomers in Subsect. 3.5, and plasmon excitations in Subsect. 3.6. Conclusions are given in Sect. 4.

2 Theory

2.1 The background

The jellium model consists of interacting electrons and a positive background charge. In an infinite system both the electron density and the background density are homogeneous and equal in magnitude. Conventionally, the jellium surface is defined as a sharp surface (step function) of the positive background charge. Then the electron density "spills out" slightly from the background, which results in a dipole layer at the surface.

Since the pioneering work of Lang and Kohn [26], the jellium model has been used to describe metal surfaces [26, 27], vacancies and voids in metals [28, 29] and metal clusters [2–5, 11]. The model describes surprisingly well (nearly quantitatively) the energetics of these systems in the case of low-density alkali metals, but fails in the case of high-density metals, such as aluminium, where it gives negative surface energies. The plain jellium model describes best sodium and potassium, where the electron density is closest to the minimum total energy value of a homogeneous electron gas.

For an accurate description of other metals, the structure of the ionic backgroud has to be taken into account. In most metals the average electrostatic potential in the pseudopotential lattice is nonzero [29]. The resulting correction can be adequately calculated in first-order perturbation theory. Several different methods for including ionic corrections in the jellium model have been proposed in the literature [17, 26, 27]. These corrections usually rely on the high symmetry of the system, as in the cases of spherical clusters, voids, and plane surfaces. The inclusion of the ionic corrections becomes much more cumbersome if the symmetry (geometrical shape) of the electron density is allowed to change during the search for the energy minimum.

The applications of the jellium model to nonspherical clusters have not included the ionic corrections. The deformations have been implemented by changing the shape of the homogeneous background charge. In their careful study of spheroidal jellium clusters, Ekardt and Penzar [11] found a qualitative explanation for the odd-even staggering and the splitting of the plasmon resonance. With more general deformations, however, the sharp edge of the background causes numerical problems. Hirschmann et al. [15] circumvented this problem by replacing the sharp edge by a diffuse one (Fermi function). If the density of the positive background is allowed to change freely, one ends up with a model where the positive background density is everywhere the same as the electron density. In our present approach we have such a completely relaxable jellium background.

2.2 The ultimate jellium model

In our model the density of the positive background charge is a function of the position. It is free to relax to any form which minimizes the total energy. The background charge has an infinite mass (compared to the valence electrons) and an internal Coulomb energy. To begin with, we show that the number density of the background, $n_{\mathrm{bg}}(\mathbf{r})$, is everywhere the same as the total electron density $n(\mathbf{r})$. In the spin-dependent density-functional formalism the total energy can be written as a functional of the spin-up and spin-down electron densities, $n_\uparrow$ and $n_\downarrow$, and the background density or, alternatively, as a functional of the total electron density $n = n_\uparrow + n_\downarrow$, the spin polarization $\zeta = (n_\uparrow - n_\downarrow)/n$, and the total charge density $\rho = e(n_{\mathrm{bg}} - n)$:

$$E[n, \zeta, \rho] = T[n, \zeta] + E_{\mathrm{xc}}[n, \zeta] + E_C[\rho], \tag{1}$$

where T, E_{xc}, and E_C are the kinetic energy, the exchange-correlation energy, and the Coulomb energy of the total charge density, respectively. Minimizing the energy functional with respect to ρ and using the constraint that the total charge be fixed (Lagrange multiplier λ), we have

$$\frac{\delta}{\delta\rho(\mathbf{r})}\left(E_C[\rho] - \lambda \int \mathrm{d}^3 r\, \rho(\mathbf{r})\right) = 0, \tag{2}$$

whence

$$\frac{1}{4\pi\varepsilon_0}\int \mathrm{d}^3 r' \frac{\rho(\mathbf{r}')}{|\mathbf{r} - \mathbf{r}'|} = \lambda. \tag{3}$$

This equation can be satisfied only if $\rho(\mathbf{r}) = 0$ and $\lambda = 0$. The charge neutrality is what one would expect

intuitively. Thus there is no Coulomb energy and the background density equals the electron density, $n_{bg} = n$. Equation (3) also gives the result that ionized clusters cannot be described on our model; the extra positive charge would escape into the vacuum.

The remaining part of the density functional (1) is minimized using the Kohn-Sham method [30] with the local-spin-density approximation for the exchange-correlation energy (for a review see [31]). The density for electrons with spin σ is written as a sum of occupied single-electron states ψ_i^σ,

$$n_\sigma(\mathbf{r}) = \sum_{i=1}^{N_\sigma} |\psi_i^\sigma(\mathbf{r})|^2, \tag{4}$$

where N_σ is the number of electrons with spin σ. Minimizing the energy functional with respect to ψ_i^σ leads to the usual Kohn-Sham equations

$$-\frac{\hbar^2}{2m} \nabla^2 \psi_i^\sigma(\mathbf{r}) + V_{xc}^\sigma(n(\mathbf{r}), \zeta(\mathbf{r}))\, \psi_i^\sigma(\mathbf{r}) = \varepsilon_i^\sigma\, \psi_i^\sigma(\mathbf{r}), \tag{5}$$

where V_{xc}^σ is the local exchange-correlation potential. We use the Perdew-Zunger parametrization [32] of the Ceperley-Alder [33] correlation energy. Equations (5) and (4) have to be solved self-consistently, and $N_\uparrow$ and $N_\downarrow$ ($N = N_\uparrow + N_\downarrow$) have to be chosen so that the total energy is minimized. In practice, it turns out that for even N we have $N_\uparrow = N_\downarrow$ and for odd N we have $N_\uparrow = N_\downarrow + 1$. Note that, due to the complete charge neutrality, the Coulomb potential or energy does not show up in the computations.

The linear Schrödinger equations (5) were solved in each iteration by using the plane-wave basis

$$\phi_{\mathbf{k}} = L^{-3/2} e^{i\mathbf{k}\cdot\mathbf{r}}, \quad \mathbf{k} = \frac{2\pi}{L}(n_1, n_2, n_3), \tag{6}$$

where $n_i = K, K-1, \ldots, -K$, the integer K determining the number of plane waves. In coordinate space we use $4K + 1$ points per axis with spacing $L/(4K + 1)$.

The iteration is started by making initial guesses for the effective potential (V_{xc}^σ) at the lattice points; we used the same initial potential for both spins. Then the fast Fourier transform (FFT) is used to expand the potentials in the plane-wave basis, and the Hamiltonian matrices are computed. After diagonalization of the Hamiltonian, the densities of the spin-up and spin-down electrons are determined from the single-electron eigenfunctions, and the FFT is again used for getting the densities at the lattice points. New effective potentials are obtained from the densities (this is where the spin-up and spin-down electrons interact), and the whole procedure is repeated until convergence is obtained. No symmetry restrictions are used.

The following steps were taken to make the computation efficient. During each iteration the center of mass and the principal axes of inertia were determined. The cluster was then moved to the origin and rotated so that the principal axes corresponding to the two smallest moments of inertia were in the $(1,1,1)$ and $(1,-1,0)$ directions, respectively. This method minimizes the electron density at the boundary of the computation box and thus minimizes the size of the box needed.

The size of the box and the number of plane waves were chosen so that the accuracy of the total energy per electron was better than or about 0.5 meV. In the final calculations for $N = 2$–8 we had $L = 35a_0$ and $K = 5$ ($11 \times 11 \times 11 = 1331$ plane waves); for $N = 9$–20, we had $L = 40a_0$ and $K = 5$; and for $N = 21$–22, we had $L = 48a_0$ and $K = 6$. These small numbers of plane waves are sufficient because the effective potential and the electron density are very smooth functions in the present model. The accuracy of the computations was checked by performing separate calculations in the spherical cases, where the system reduces to a mathematically one-dimensional problem.

For each cluster the iteration was started from four different initial potentials. These were selected to represent the basic geometries the clusters were expected to have; sphere, prolate and oblate spheroid, and a pear shape (octupole deformation). In each case, random perturbations without any symmetry were added to the initial potential for ensuring that the system had the possibility of reaching other symmetries than the initial guess.

From each initial potential the equations were iterated to full convergence. When the solution has inversion symmetry, this takes about 50 iterations. Solutions with broken inversion symmetry were more difficult to find (see Subsect. 3.3). At most two different converged solutions were obtained for any of the small clusters studied (up to $N = 22$). We call them "ground state" and "isomer" according to their total energy. In many cases only one solution was found, irrespective of the initial guess for the effective potential.

We found the plane-wave basis very well suited to the present model where the electron density, the potential, and the wave functions vary slowly. The equations can also be solved directly by using a cubic grid in coordinate space. This method has been used for the smallest clusters by Manninen [34]. However, for getting the same accuracy, one needs many more lattice points than one needs plane waves, if only the nearest neighbors are used to estimate the Laplace operator ∇^2. Chelikowsky et al. [35] have recently suggested that the real-space technique can be improved through a better description of ∇^2. It is likely that this technique could be used successfully in the ultimate jellium model.

2.3 Deformation parameters and moments of inertia

The electron densities are analyzed and displayed in the principal axes of inertia. We choose the z axis to be that of the greatest symmetry of the cluster. This is done in the following way. The three moments of inertia are

$$I_i = M \int d^3 r (r^2 - x_i^2)\, n(\mathbf{r}), \tag{7}$$

where M is the atomic mass. We now normalize the I_i so that their sum is 3, i.e., we replace them by $\mathcal{I}_i = 3I_i / \sum_j I_j$. Then clusters with two moments of inertia greater than 1 (prolate types) are placed to have the smallest moment

along the z axis and the largest one along the x axis. Those with two moments smaller than 1 (oblate types), are placed to have the largest moment along the z axis and the smallest along the x axis.

In the cases where inversion symmetry is broken, these rules cannot completely define the orientation of the cluster. The remaining freedom is not important for determining the deformation parameters, and the orientation is chosen to make the figures the most informative.

We note here that the total energies, single-particle energies, and moments of inertia are obtained from the original electron densities calculated by the primary computer code (using $4K + 1$ points per axis). The final electron density was stored with only $2K + 1$ points per axis. This smaller accuracy was used in computing the multipole moments, plasmon energies, and contour plots of the energy. However, the results are correct within the accuracy given in the tables.

The shape of the cluster was analyzed in terms of a multipole expansion. We define the number multipole moments Q_{lm} as [36]

$$Q_{lm} = \sqrt{\frac{4\pi}{2l+1}} \int \mathrm{d}^3 r\, r^l Y_{lm}(\theta, \phi)\, n(\mathbf{r}), \tag{8}$$

where Y_{lm} is a spherical harmonic. The somewhat unusual normalization appearing here has the convenient feature that $Q_{00} = N$, the number of electrons. Multipole moments Q_{lm} with different l have diffeent dimensions and therefore cannot be compared. It is then more informative to use dimensionless shape parameters a_{lm} defined as

$$a_{lm} \equiv \frac{\sqrt{4\pi(2l+1)}}{3 r_s^l N^{l/3+1}} (Q_{lm} - \delta_{l0} N), \tag{9}$$

where we use the electron-gas bulk value $r_s = 4.18 a_0$.

We arrived at the scaling formula (9) as follows. The surface of a homogeneous body can be described by the expansion

$$R(\theta, \phi) = R_0 \left[1 + \sum_{lm} a_{lm} Y_{lm}^*(\theta, \phi) \right]. \tag{10}$$

This equation is used in nuclear physics for the description of the surface of a deformed nucleus [37, 38]. In the present context, we identify $R_0 = r_s N^{1/3}$ and keep the density constant at $n = (\frac{4}{3}\pi r_s^3)^{-1}$. When one calculates the multipole moment Q_{lm} from (8) for this *homogeneous* distribution, the result agrees with (9) *to first order in the coefficients* a_{lm}. Equation (9), on the other hand, defines an *exact* scaling of the Q_{lm} of (8) irrespective of the contents of (10).

In spite of its approximate nature in relation to (8) and (9), (10) does give an indication of the shape of the cluster. Furthermore, various general properties of the a_{lm} can be deduced from (10) with full validity. Thus the reality of $R(\theta, \phi)$ implies that $a_{l,-m} = (-1)^m a_{lm}^*$, so we only need to give the moments with $m \geq 0$. From (9) we have $a_{00} = 0$. The center of mass is kept fixed at the origin, whence $a_{1m} = 0$. Furthermore, we choose to orient the cluster so that its quadrupole shape lies in a set of principal axes. Then the a_{2m} are real with $a_{2\pm1} = 0$ and $a_{22} = a_{2,-2}$. It is important to note that the orientation of the principal axes is independent of the deformations $l \neq 2$.

Specific symmetries of the cluster impose further conditions on the a_{lm} coefficients. For spherical symmetry all coefficients are zero. For axial symmetry all coefficients with $m \neq 0$ are zero, and for inversion symmetry all coefficients with odd l are zero.

We have calculated the a_{lm} coefficients up to $l = 6$. Even the higher multipoles seem to be important in many cases. Unfortunately they cannot be calculated accurately because of the dominating r^l factor in (8), and the fact that the electron densities do not exactly reach zero at the boundaries of the computation box.

With the shape parameters a_{20} and a_{22} at our disposal, we can also determine the deformation parameters β and γ common in nuclear physics [37, 38]:

$$a_{20} = \beta \cos\gamma,\ a_{22} = \frac{1}{\sqrt{2}} \beta \sin\gamma. \tag{11}$$

For given values of a_{20} and a_{22} we can find a unique pair β and γ when we impose the constraints $\beta \geq 0$ and $0 \leq \gamma < 2\pi$. Here β gives the magnitude of the quadrupole deformation and γ gives its detailed shape and orientation. In fact, the interval $0° \leq \gamma \leq 60°$ already contains all possible quadrupole shapes; the remaining values of γ only repeat them in different orientations. Therefore we also tabulate $\gamma_{\mathrm{eff}} \in [0, \pi/3]$, which can be obtained from γ by a simple reflection technique. The values $\gamma_{\mathrm{eff}} = 0°$, $30°$, and $60°$ mean axial prolate, maximal triaxiality, and axial oblate, respectively.

The moments of inertia are obviously related to the quadrupole moments Q_{2m} of (8). The exact relations are

$$\begin{aligned}
I_x &= \frac{M}{3}\left[2\int \mathrm{d}^3 r\, r^2 n(\mathbf{r}) + Q_{20} - \sqrt{6}\, Q_{22} \right], \\
I_y &= \frac{M}{3}\left[2\int \mathrm{d}^3 r\, r^2 n(\mathbf{r}) + Q_{20} + \sqrt{6}\, Q_{22} \right], \\
I_z &= \frac{M}{3}\left[2\int \mathrm{d}^3 r\, r^2 n(\mathbf{r}) - 2Q_{20} \right],
\end{aligned} \tag{12}$$

where we have used $Q_{2,-2} = Q_{22}$. The Q_{2m} can be exactly replaced by the a_{2m} according to (9). We note that deformations other than $l = 2$ only contribute to the scalar integral term, which is the same for I_x, I_y, and I_z. Accordingly the *dynamical* deformation is entirely due to $l = 2$.

In the rough approximation of a uniform density and a small deformation, as discussed in connection with (10), the integral in (12) becomes $\frac{3}{5} N R_0^2$, and we have for the moments of inertia

$$\begin{aligned}
I_x &\approx \frac{2}{5} N M R_0^2 \left(1 + \sqrt{\frac{5}{16\pi}}\, a_{20} - \sqrt{\frac{15}{8\pi}}\, a_{22} \right), \\
I_y &\approx \frac{2}{5} N M R_0^2 \left(1 + \sqrt{\frac{5}{16\pi}}\, a_{20} + \sqrt{\frac{15}{8\pi}}\, a_{22} \right), \\
I_z &\approx \frac{2}{5} N M R_0^2 \left(1 - \sqrt{\frac{5}{4\pi}}\, a_{20} \right).
\end{aligned} \tag{13}$$

The leading term in these expressions is the elementary result for a sphere. We have not used them quantitatively, since in many cases they would be very bad approximations. Nevertheless, they serve to visualize the dynamics of deformation. The factors in parentheses are seen to be approximations for the normalized moments of inertia $\mathscr{I}_i$ introduced after (7).

2.4 Plasmon excitation

In metal clusters the photoabsorption cross section is dominated by the plasmon excitation. In jellium clusters the classical Mie plasmon peak is split into several peaks due to Landau damping [39] and to deformation away from spherical shape [9, 10]. Here we only study the effect of deformation. In a nonspherical cluster the plasmon peak splits into two or three peaks depending upon the symmetry.

We estimate the plasmon energies in the ultimate jellium model by means of a simple classical approximation. (This gives the same result as the sum-rule approach presented in [2].) The Coulomb energy of the electrons, of density $n(\mathbf{r})$, in the ionic background potential $V_{\mathrm{bg}}(\mathbf{r})$ is

$$E_C = -e\int \mathrm{d}^3 r\, V_{\mathrm{bg}}(\mathbf{r})\, n(\mathbf{r}). \tag{14}$$

Let $i = 1, 2, 3$ label the inertial principal axes of the cluster. If we now displace the electron cloud as a whole by $\hat{\mathbf{e}}_i \Delta x_i$, the energy change is, to order $(\Delta x_i)^2$,

$$\begin{aligned}\Delta E_C &= -e\int \mathrm{d}^3 r\, V_{\mathrm{bg}}(\mathbf{r})\,[n(\mathbf{r}-\hat{\mathbf{e}}_i\Delta x_i) - n(\mathbf{r})] \\ &= -\frac{e}{2}(\Delta x_i)^2 \int \mathrm{d}^3 r\, V_{\mathrm{bg}}(\mathbf{r})\,\frac{\partial^2}{\partial x_i^2}\, n(\mathbf{r})\end{aligned} \tag{15}$$

Note that the first-order term vanishes because of equilibrium and $\partial^2 n/\partial x_i^2$ is predominantly negative. We equate ΔE_C to the harmonic potential energy $\frac{1}{2} N m w_i^2 (\Delta x_i)^2$ for vibrations in the x_i direction. The corresponding plasmon energy is then

$$\hbar w_i = \left[-\frac{e\hbar^2}{Nm} \int \mathrm{d}^3 r\, V_{\mathrm{bg}}(\mathbf{r})\,\frac{\partial^2}{\partial x_i^2}\, n(\mathbf{r}) \right]^{1/2} \tag{16}$$

This result is generaly valid insofar as it is a good approximation to consider the electron cloud as oscillating rigidly against the positive ionic background. Only the inertial ellipsoid affects the frequencies [40]. In our particular case, the equilibrium Coulomb energy E_C is zero and the background density is the same as the electron density.

In the case of a conventional spherical jellium cluster, (16) leads to the so-called spillout formula [2]. The spillout formula overestimates the plasmon energy as compared to time-dependent LDA [41], radom-phase approximation (RPA) [39], or CI [42] calculations, which take dynamical screening into account.

3 Results

3.1 Ground-state geometries

The ground-state electron densities of the clusters with 2 to 22 electrons are shown in Figs. 1, 2, and 3. For each cluster we show a three-dimensional plot of a constant-density surface with density $n = 0.00125 a_0^{-3}$ (38% of bulk density) and contour plots of the electron density in the yz, xz, and xy planes. The contour corresponding to the second-lowest density is the one used for making the three-dimensional plots.

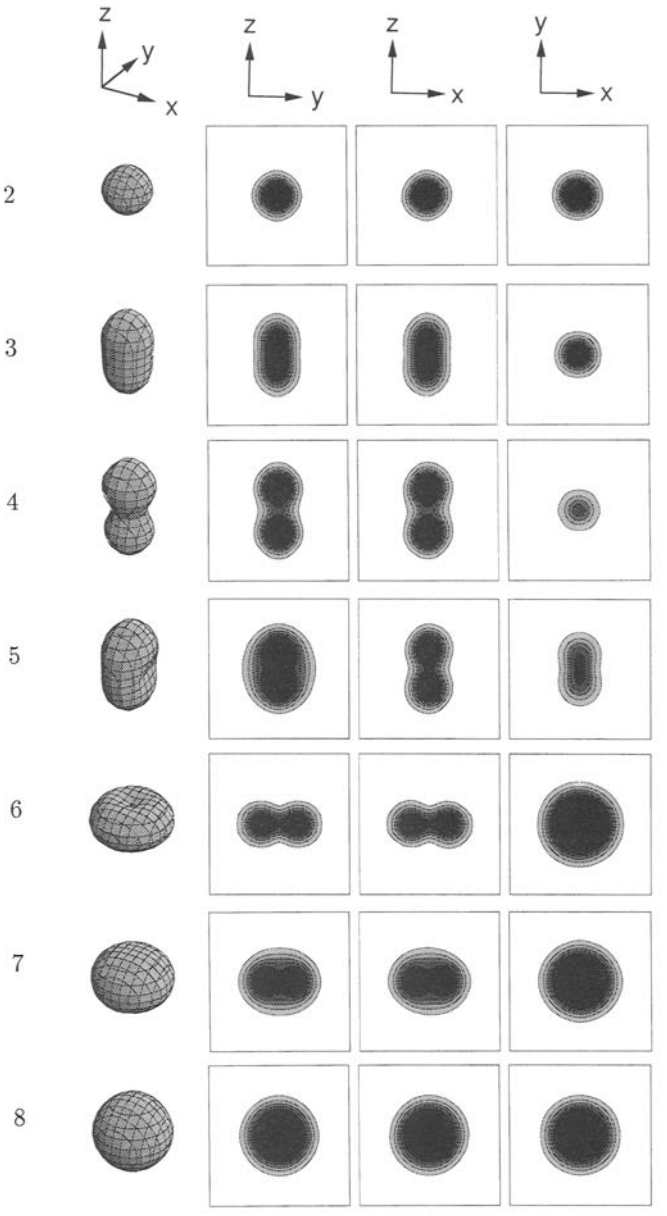

Fig. 1. Ground-state densities for clusters with 2 to 8 electrons. The coordinate system is shown at the *top* of the figure. The three-dimensional plots are constant-density surfaces with density $n = 0.00125 a_0^{-3}$ (38% of bulk density). The three-dimensional figures do not have an absolute length scale. The two-dimensional contour plots show the electron densities in the yz, xz, and xy planes. The five contour lines range from $n = 0.0006 a_0^{-3}$ (18% of bulk density) to $n = 0.0032 a_0^{-3}$ (98% of bulk density) with equal spacing. The contour for the second-lowest density is the one used for making the three-dimensional plots. The side of each square is $31 a_0$, which puts the contour plots on an absolute scale

The clusters with 2, 8, 19, and 20 electrons are spherical, whereas all the others are deformed. The clusters with

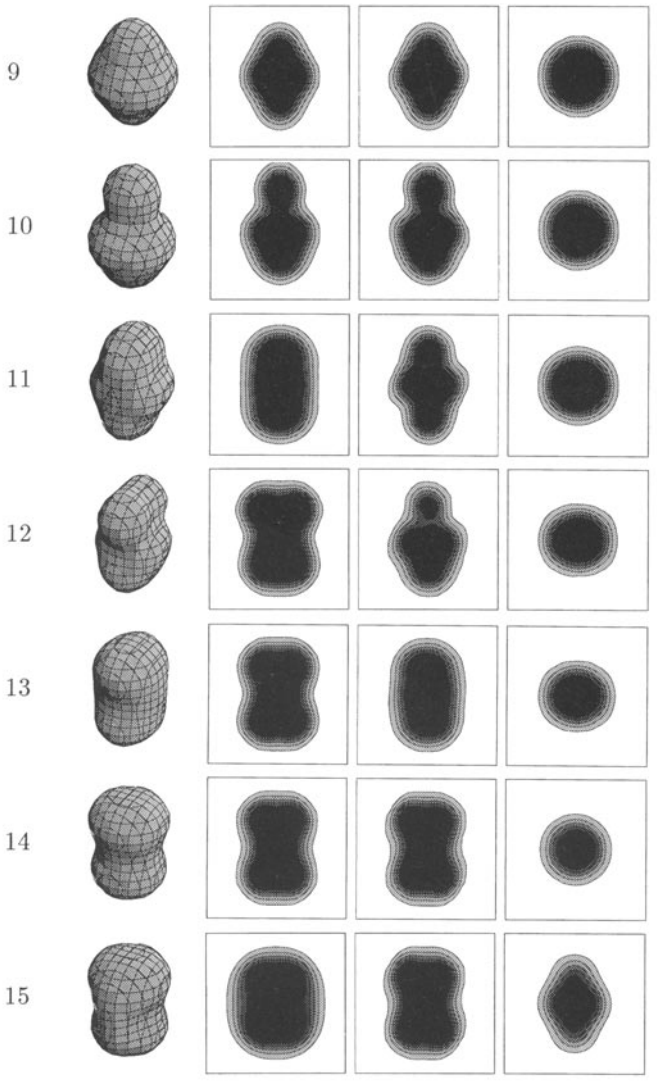

Fig. 2. Ground-state electron densities for clusters with 9 to 15 electrons. For details see Fig. 1

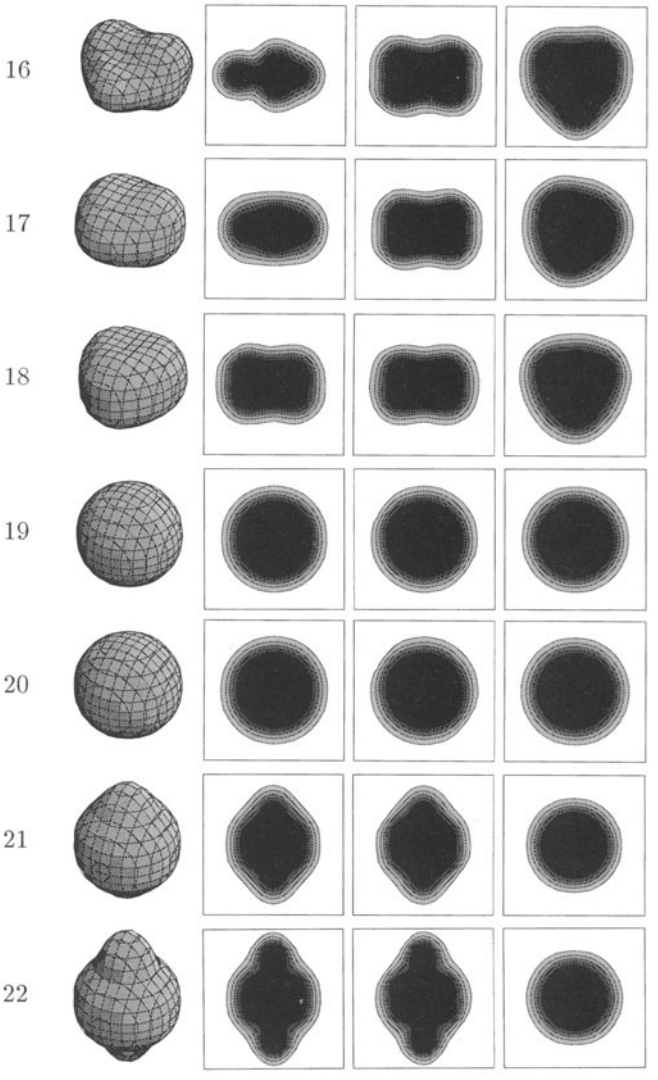

Fig. 3. Ground-state electron densities for clusters with 16 to 22 electrons. The side of the square surrounding the 21- and 22-electron clusters is $35a_0$. Other details are as given in Fig. 1

3, 4, 6, 7, 9, 14, 21, and 22 electrons have axial and inversion symmetry. The 10-electron cluster has only axial symmetry, and the 5-, 11-, 13-, and 15-electron clusters have only inversion symmetry. The clusters with 12, 16, 17, and 18 electrons have neither inversion nor axial symmetry.

The geometries of the smallest clusters can be easily understood in terms of the symmetries of the s, p_x, p_y, p_z, etc. single-particle wave functions of a spherical system [34]. In the spherical case all the p levels are degenerate, but in a deformable system the Jahn-Teller effect splits them unless the l shell is full. Although l ceases to be a good quantum number as deformation sets in, we can refer to the wave function as p_x type etc. according to its unperturbed symmetry.

In our simple view, the two-electron cluster is spherical due to the two s electrons. The clusters with three and four electrons have one or two p_z-type electrons and consequently the electron density is axially symmetric and prolate. Reserving z to be the symmetry axis also for oblate shape, we can now relabel the p levels so that the third and fourth electrons fill the p_x levels and the fifth electron goes into p_y, which results in a triaxial five-electron cluster. Then in the six-electron cluster both p_x and p_y are full. This cluster has oblate axial symmetry, as can be seen from Fig. 1. The seventh electron now occupies the p_z level and the cluster stays axially symmetric. The eighth electron completes the p shell and the cluster is again spherical.

The geometries of the clusters with 9 to 20 electrons can be understood in terms of filling the d- and $2s$-type levels. However, due to the strong deformations in the middle of the shell, the situation is now more complex. A simple explanation is available near the magic numbers. The nine-electron cluster has one d electron and is axially symmetric and prolate. The 19- and 20-electron clusters have a full d shell plus one and two $2s$ electrons, respectively. Both of them are spherically symmetric. The ground state of the 18-electron cluster is nonspherical due to a mixing of the d and $2s$ levels. However, the 18-electron

cluster has a spherical isomer (with a full d shell) which is practically degenerate with the ground state (see Subsect. 3.5).

Special attention should be paid to the 14-electron cluster. Although it is strongly deformed, its large binding energy qualifies it as semimagic. It has axial and inversion symmetry.

Finally, the shapes of the 21- and 22-electron clusters can be qualitatively understood as resulting from one and two f-type electrons, respectively, outside the 20-electron magic core.

Figure 4 shows the normalized principal moments of inertia $\mathscr{I}_i$ of the cluster ground states (black dots). For the spherical clusters with $N = 2$, 8, 19, and 20, all moments are equal to 1. For prolate and oblate shapes, respectively, two of the moments are > 1 and < 1. For clusters without axial symmetry, generally all three moments of inertia are different. An exception is the 18-electron cluster, which has D_3 symmetry.

Qualitatively, cluster shape as a function of the number of electrons has a clear pattern: at the beginning of a shell the shape is prolate and at the end it is oblate. The same result has been obtained with the ellipsoidal jellium models [11, 12], and also with more general jellium-type models [13, 15] and the simple Hückel model [43, 44]. This pattern, however, is expected to change after $N = 40$ so that the shape is oblate at the beginning of a shell and prolate at the end [13, 15].

We have analyzed the cluster shapes in terms of a multipole expansion as explained in Subsect. 2.3. Table 1 gives the deformation parameters β, γ, and γ_{eff} calculated from (9) and (11). All shape parameters a_{lm} are calculated from (9). They are given in Tables 2–5, organized in order of decreasing symmetry. The spherical clusters are not shown in the tables since for them all the a_{lm} are zero. Likewise the tables omit other a_{lm} that are systematically zero.

The coefficients for clusters with both axial and inversion symmetry are given in Table 2. The importance of

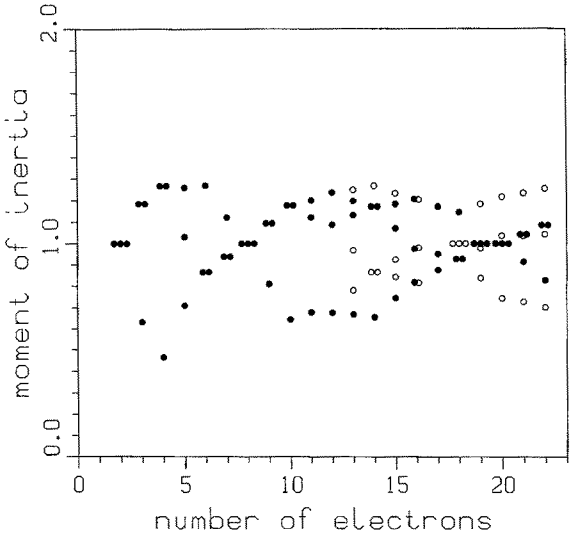

Fig. 4. Moments of inertia for the ground states (*black dots*) and isomers (*open circles*). The sum of the three moments is normalized to be unity

Table 1. Calculated energies and quadrupole deformation parameters for ground states and isomeric states

N	E/N (eV)	β	γ (°)	γ_{eff} (°)
2	−1.7946	0.000	0.0	0.0
3	−1.7207	0.936	0.0	0.0
4	−1.8190	1.460	0.0	0.0
5	−1.7926	0.729	335.6	24.4
6	−1.8528	0.554	180.0	60.0
7	−1.8623	0.223	180.0	60.0
8	−1.9182	0.000	0.0	0.0
9	−1.8899	0.342	0.0	0.0
10	−1.9082	0.707	0.0	0.0
11	−1.8963	0.627	351.9	8.1
12	−1.9117	0.662	345.2	14.8
13	−1.9115	0.643	353.3	6.7
14	−1.9304	0.665	0.0	0.0
15	−1.9209	0.486	345.6	14.4
16	−1.9336	0.412	156.1	36.1
17	−1.9344	0.309	165.9	45.9
18	−1.9490	0.249	180.0	60.0
19	−1.9547	0.000	0.0	0.0
20	−1.9688	0.000	0.0	0.0
21	−1.9571	0.140	0.0	0.0
22	−1.9618	0.289	0.0	0.0
13*	−1.9050	0.516	156.6	36.6
14*	−1.9234	0.498	180.0	60.0
15*	−1.9200	0.431	168.5	48.5
16*	−1.9336	0.411	155.1	35.1
18*	−1.9486	0.000	0.0	0.0
19*	−1.9389	0.355	156.1	36.1
20*	−1.9455	0.508	337.7	22.3
21*	−1.9419	0.539	337.1	22.9
22*	−1.9488	0.600	337.7	22.3

$l = 4$ and 6 is evident. Our calculations show that even higher multipole moments are significant. Unfortunately, we can determine the coefficients accurately only up to $l = 6$.

Table 3 shows the shape coefficients for the one cluster, $N = 10$, which is axially symmetric but lacks inversion symmetry. Table 4 gives the results for clusters with inversion symmetry but no axial symmetry, and Table 5 gives the results for clusters which lack both inversion and axial symmetry.

In all cases the coefficients with even l are real and their odd-m components are zero. This implies that the even-l deformations are always symmetrically oriented with respect to the principal axes. Also the odd-l coefficients, in Tables 3 and 5, show a systematic behavior: their even-m components are real and odd-m components complex.

3.2 *Cluster molecules*

Some of the cluster shapes in Figs. 1–3 can be interpreted as "molecules" built up from magic clusters. This is illustrated in Fig. 5. The four-electron cluster consists of two dimers, with a separation energy of only 97 meV. The 10-electron cluster consists of an eight-electron sphere with a dimer attached to it, with a separation energy of 147 meV.

The 12-electron cluster is interpreted as two dimers attached to an eight-electron cluster. The energy needed

Table 2. Shape coefficients for clusters with both axial and inversion symmetry

N	3	4	6	7	9	14	21	22	14*
a_{20}	0.94	1.46	−0.55	−0.22	0.34	0.67	0.14	0.29	−0.50
a_{40}	0.62	1.16	0.21	0.04	0.36	−0.01	0.18	0.41	0.32
a_{60}	0.39	0.84	−0.08	−0.01	0.25	−0.20	0.16	0.44	−0.19

Table 3. Shape coefficients for the cluster with axial symmetry but without inversion symmetry

N	10
a_{20}	0.71
a_{30}	0.45
a_{40}	0.90
a_{50}	0.71
a_{60}	1.03

to separate these three building blocks is 416 meV. Since the two dimers on the surface of the eight-electron cluster come close to forming a four-electron cluster, we can estimate the separation energy as follows. First, we separate the four-electron cluster on the surface of the eight-electron cluster into two dimers. This requires 97 meV when we assume that the eight-electron cluster does not change the dimer binding energy. Then we separate the two dimers from the eight-electron cluster. This requires 2×147 meV. The resulting total separation energy is 391 meV, in reasonable agreement with the exact value of 416 meV.

The 16-electron cluster can be interpreted as a composite of the strongly deformed, yet very stable, 14-electron cluster and a dimer. The separation energy is 322 meV, which is so large that the molecular interpretation must be taken cautiously.

The tendency to these molecular structures is due to the very strong binding of the dimer in the ultimate jellium model.

3.3 Softness of the ground state

All clusters lacking inversion symmetry are extremely soft against odd-l deformations. These are the clusters with 10, 12, 16, 17, and 18 electrons, shown in Figs. 2 and 3.

Consider the case of the 10-electron cluster. Its pear-shaped ground state is obtained easily only when the initial potential has the same symmetry. Our three other initial potentials (sphere, oblate and prolate spheroids) produce a more complicated convergence to the ground state. Within about 30 iterations each of these initial potentials produces the same "intermediate" state. It is prolate, with axial and inversion symmetry, and closely resembles the ground state of the 9-electron cluster. Within the next 300 iterations the intermediate state transforms slowly to the pear-shaped ground state. The energy surface between these two geometries is nearly constant: the energy is continuously lowered by a total of only 0.5 meV/electron. The intermediate state can be viewed as a saddle point on the energy surface.

Related softness of the pear shape has been observed in nuclear physics [38, 45]. In the absence of the infinitely heavy ionic background we could interpret our 10-electron cluster as an octupole vibrator, where the pear shape oscillates back and forth through the intermediate state. In nuclear physics there is well-established experimental evidence of octupole vibrators, but only weak evidence of static octupole deformation in the ground state [45].

A similar intermediate state with inversion symmetry was observed also in all other clusters where the ground state lacks inversion symmetry. In a few tens of iterations the density converges to the symmetric intermediate state. Then it takes hundreds of iterations to break the inversion symmetry, and the energy is lowered in this process very little, usually even less than in the case of the 10-electron cluster. It should be noted that, due to random perturbations, the intermediate state is obtained regardless of the symmetries of the initial potential.

In some clusters, the energy minimum in phase space is evidently so flat that one can speak of a "ground-state area". This includes all shapes with nearly the same energy and no barrier between them. The ground-state area includes not only the intermediate state and the ground state, but also all shapes in between.

A good example is the 16-electron cluster. Its ground state can be viewed as a 14-electron cluster with a dimer attached to it. In the intermediate state the density of the

Table 4. Shape coefficients for clusters with inversion symmetry but without axial symmetry

N	5	11	13	15	13*	15*	21*	22*
a_{20}	0.66	0.62	0.64	0.47	−0.47	−0.42	0.50	0.56
a_{22}	−0.21	0.06	−0.05	−0.09	0.15	0.06	−0.15	−0.16
a_{40}	0.29	0.41	0.06	−0.04	0.31	0.19	0.45	0.40
a_{42}	−0.11	0.17	−0.14	0.01	−0.10	0.05	−0.04	−0.12
a_{44}	0.06	0.01	0.01	0.05	−0.08	0.01	−0.01	−0.01
a_{60}	0.11	0.24	−0.13	−0.11	−0.18	−0.08	0.38	0.18
a_{62}	−0.06	0.16	−0.12	0.04	0.06	−0.04	−0.09	−0.22
a_{64}	0.03	0.03	0.02	0.03	0.03	0.01	−0.01	0.00
a_{66}	−0.02	0.00	0.00	−0.02	−0.04	0.00	0.02	0.01

Table 5. Shape coefficients for clusters with no inversion symmetry and no axial symmetry

N	12	16	17	18	16*	19*	20*
a_{20}	0.64	−0.38	−0.30	−0.25	−0.37	−0.33	0.47
a_{22}	−0.12	0.12	0.05	0.00	0.12	0.10	−0.14
a_{30}	0.05	0.00	0.00	0.00	0.00	0.00	0.00
a_{31}	0.00	−0.03i	−0.01 − 0.01i	0.00	−0.02	0.01i	−0.18i
a_{32}	−0.09	0.00	0.00	0.00	0.00	0.00	0.00
a_{33}	0.00	0.02 − 0.16i	−0.07 − 0.05i	−0.01 − 0.11i	−0.15 − 0.02i	−0.14i	−0.03i
a_{40}	0.15	0.09	0.01	−0.05	0.09	0.04	0.51
a_{42}	−0.33	0.11	0.05	0.00	0.10	−0.08	0.02
a_{44}	0.02	0.03	0.00	0.00	0.01	0.12	−0.02
a_{50}	−0.07	0.00	0.00	0.00	0.00	0.00	0.00
a_{51}	0.00	0.04i	0.01 + 0.01i	0.00	0.04 + 0.01i	−0.01i	−0.10i
a_{52}	−0.14	0.00	0.00	0.00	0.00	0.00	0.00
a_{53}	0.00	−0.01 + 0.06i	0.01 + 0.01i	0.00	0.06 + 0.01i	0.01i	0.00
a_{54}	0.03	0.00	0.00	0.00	0.00	0.00	0.00
a_{55}	0.00	−0.01 + 0.05i	0.01 + 0.01i	0.00	0.04 + 0.01i	−0.04i	−0.01i
a_{60}	−0.08	−0.03	0.03	0.05	−0.03	−0.01	0.54
a_{62}	−0.29	−0.09	−0.03	0.00	−0.09	0.06	0.00
a_{64}	0.09	0.02	0.01	0.00	0.05	−0.07	−0.02
a_{66}	0.00	−0.05	0.01	−0.02	0.05	0.09	0.02

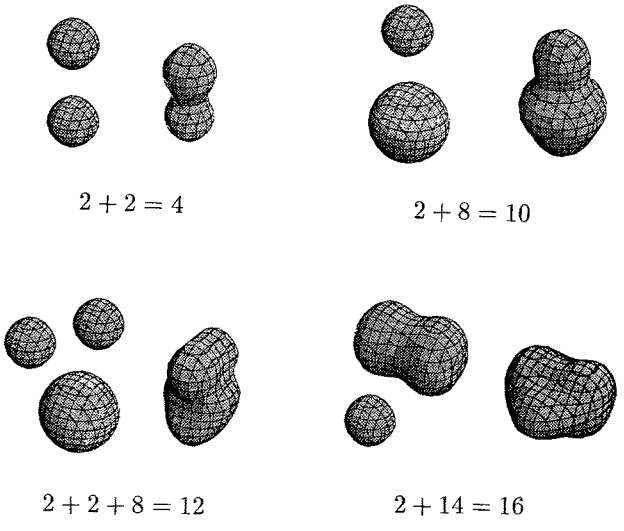

Fig. 5. Molecular interpretation of some ground-state cluster geometries

dimer is uniformly distributed in the xy plane of the axially symmetric 14-electron cluster. The intermediate state continuously transforms to the ground state in about 400 iterations. The total energy change in this process is only 0.3 meV/electron.

In one computation extending to 600 iterations, we reached yet another well-defined shape. It is denoted by 16* and shown in Fig. 8. The shape 16* was obtained after 150 iterations. During the following 450 iterations the shape started slowly to transform to the ground state. In the process, one of the bumps on the side of the 14-electron core increases and the other decreases.

The slow convergence towards the ground state is understandable since all shapes occurring in the ground-state area, viz., 16*, 16, and all shapes in between, lie within 0.4 eV/electron of each other. Since our absolute energy accuracy is about 1 meV/electron, we cannot be sure which of these shapes represents the actual ground state of the 16-electron cluster. We describe the properties of 16* in connection with the isomers, Subsect. 3.5. Nevertheless, 16* is not a genuine isomer since it can transform to the ground state without any activation energy. Rather, it is evidently akin to the intermediate saddle-point state in the $N = 10$ cluster.

The ground-state shape of the 18-electron cluster is triangular, but extremely soft against triangular deformations. The energy gain from axial to triangular symmetry is only 0.2 meV/electron. Also the $N = 6$ cluster was found to be soft against triangular deformations.

We conclude that clusters without inversion symmetry are soft against deformation so that the energy difference between the symmetric and asymmetric solution is extremely small. It is interesting to note that in these cases also the moments of inertia and some other shape parameters are very similar in symmetric and asymmetric clusters. This is seen clearly by comparing the results for the 16 and 16* clusters. Also the single-particle energy eigenvalues are similar. The only clear difference is observed in the odd-l shape parameters.

3.4 Magic numbers and odd-even staggering

The magic numbers corresponding to closed electronic shells are clearly seen in the total energies of the spherical jellium model [1, 2]. When the shape is allowed to deform, the energy of the clusters with partially filled shells decreases and consequently the effect of the magic numbers is diminished.

Figure 6 shows the total energy per electron for the ground states in the ultimate jellium model (the numerical values are listed in Table 1). The energy shows a clear odd-even staggering. It is due to the (approximate) spin degeneracy of the single-particle levels and the Jahn-Teller effect: the deformation can lift any degeneracy except the spin degeneracy [8]. To visualize the effect of the magic

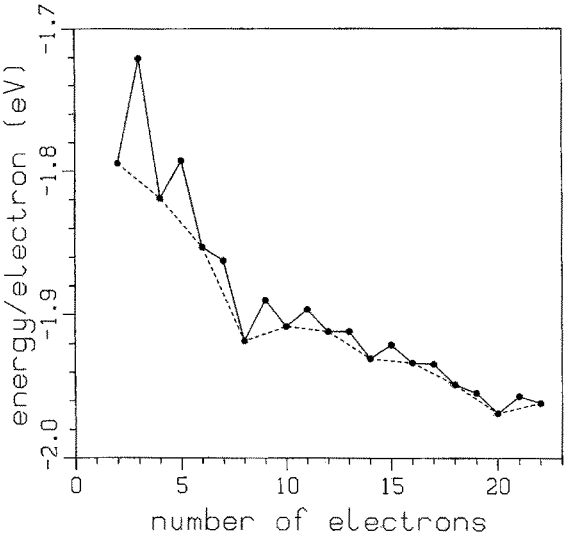

Fig. 6. The total energy per electron for the ground state. Even clusters are connected with a *dashed line* to clarify the effect of the magic numbers 8 and 20, and the semimagic number 14

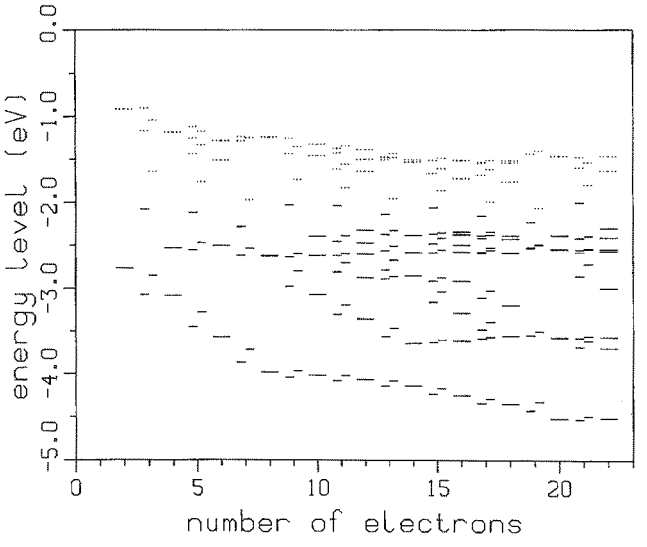

Fig. 7. Single-particle energy levels for the ground states. The lowest empty levels are shown as *dashed lines*. Spin-up and spin-down levels are given in different columns. For even clusters they are degenerate (*long lines*), whereas in odd clusters they form two separate levels (*short lines*)

numbers, we have connected the energies of the even clusters with a dashed line. There is a clear cusp at $N = 8$ and 20. Surprisingly, the strongly deformed cluster with 14 electrons also shows an enhanced stability.

Figure 7 shows the single-electron energy levels for the ground states. Spin-up and spin-down levels are shown in different columns. Above the occupied states, three empty levels are displayed by dotted lines. In even clusters the spin-up and spin-down levels are degenerate. Each odd cluster has an unpaired electron that splits the spin-up and spin-down levels. The splitting is seen to be maximal at the highest occupied molecular orbital (HOMO). Compared with the spin-independent formalism (LDA), the splitting reduces the odd-even staggering by about 30%, in agreement with the simple estimate of Manninen et al. [8].

The effect of deformation is clearly seen in the energy levels of Fig. 7. Deformation opens up a large gap at the Fermi level. The gap is almost as large for the nonmagic clusters as it is for the magic ones. This can be most easily seen by looking at the even clusters. In the odd clusters, deformation lowers the HOMO level in the middle of the gap, and the spin splitting pushes it further down.

In all clusters the $1s$-type level is clearly separated from the other levels, but the $1p$-type shell is clearly separated from other levels only at the closing of the $1d2s$ major shell, around $N = 20$.

3.5 Isomers and softness of the ground state

For clusters with 13, 14, 15, 18, 19, 20, 21, and 22 electrons we found one stable isomer for each. These are marked with an asterisk (*). An isomer represents a local minimum in the total energy, and it cannot transform to the ground state without going over an energy barrier. (As discussed in Subsect. 3.3, 16* is not a true isomer.) The shapes of the isomers are shown in Fig. 8. The moments of inertia are shown in Fig. 4 (open circles) together with those for the ground states (black dots). The total energies per electron and the quadrupole deformation parameters β and γ are given in Table 1. Grouped according to the symmetries, Tables 2, 4, and 5 give the shape parameters a_{lm} of the isomers.

The prolate clusters with 13, 14, and 15 electrons have also oblate isomers. The energies of these isomers lie within 7 meV/electron above the ground state (Table 1). We cannot determine the energy barrier between the isomer and the ground state. However, the path of convergence towards the isomeric state implies that it is much higher than the energy difference between the isomer and the ground state. The isomers 13*, 14*, and 15* (as well as the ground states 13, 14, and 15) are clearly related to each other.

The 18-electron cluster has a spherical isomer 18*. Its $1d$ shell is full and $2s$ shell empty. The electron density in the center of the cluster is only about 20% of the bulk density. The low central density appears as a hole in the contour plots of Fig. 8.

The electron densities of the spherical clusters 18* and 20 are plotted in Fig. 9. They are compared with the electron densities from the conventional jellium model with a homogeneous background charge ($r_s = 4.18a_0$). In the conventional model, the central density of 18* is smaller than the average density. In the ultimate jellium model the central density becomes even smaller because there is no Coulomb energy opposing such nonuniformity. In the case of the 20-electron cluster, where the $2s$ state is full, the situation is the opposite: the ultimate model gives a much larger density in the center than the conventional model.

The radius of the electron distribution is different in the two models. We define the radius as the distance where the density is $0.00163a_0^{-3}$, i.e., one-half of the bulk value. Figure 9 shows that the ultimate model gives a slightly

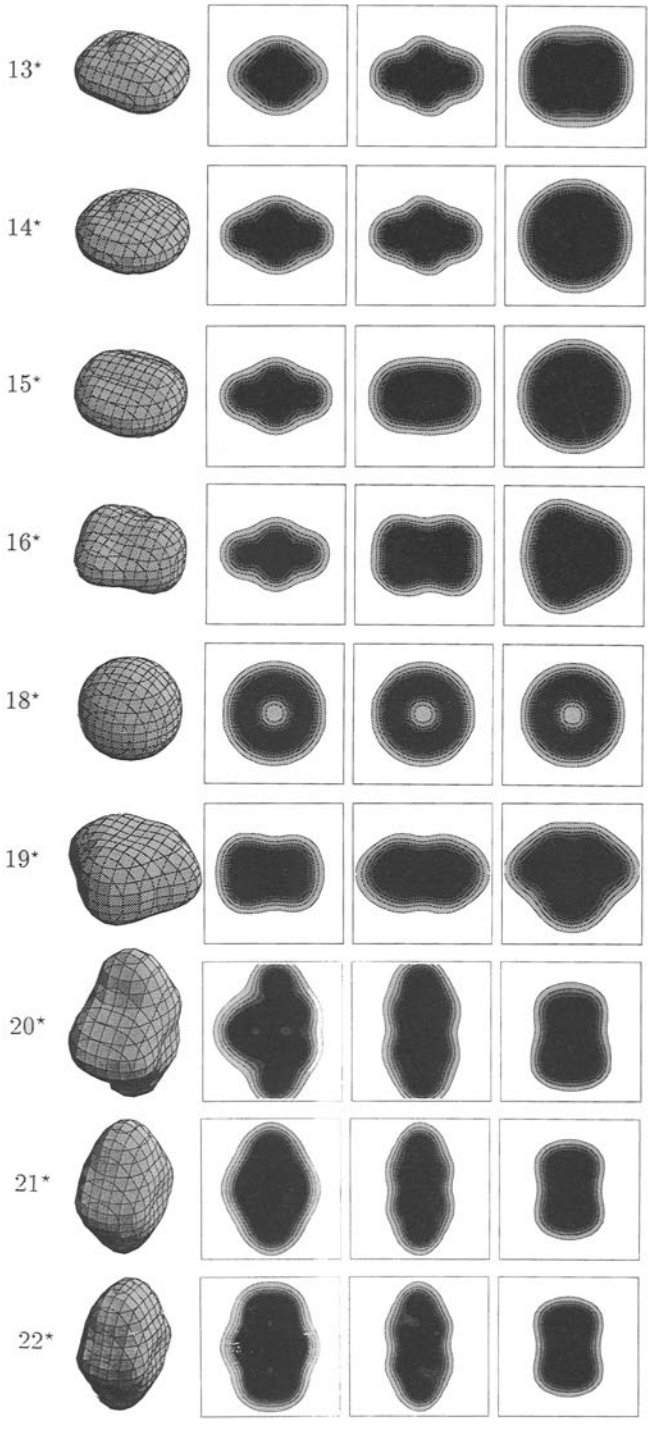

Fig. 8. Geometries of the stable isomers. The 16* is not a real isomer: it is due to a saddle point rather than a local energy minimum (see the text). For details, see Figs. 1 and 3 (note the different scale for the 21- and 22-electron clusters)

smaller radius for the electron density than does the conventional model. The reason for this is the surface tension. In the ultimate model, it can compress the cluster, whereas in the conventional model the density, and thus also the radius, are determined by the rigid background.

The isomers 19*, 20*, 21*, and 22* have shapes related to that of the ground state of the 18-electron cluster. The

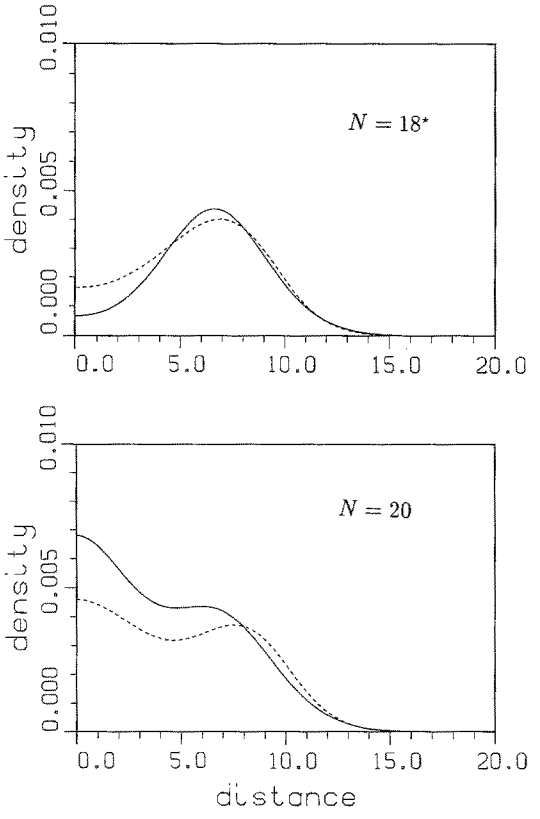

Fig. 9. Radial distribution of the electron density (in units of a_0^{-3}, radius in units of a_0) of the ultimate jellium model (*solid line*) compared with that of the conventional jellium model (*dashed line*) for the spherical isomer of the 18-electron cluster and for the spherical ground state of the 20-electron cluster

interior electron density in these clusters is very close to the density of the highest contour line in the figures. This makes the contour picture very sensitive to small variations of the density. The energies of these isomers are clearly higher than the ground-state energies, the difference being 10–20 meV/atom. The 21* and 22* are oblate whereas the $N = 21$ and 22 ground states are prolate. It is expected [13, 15] that with increasing cluster size the energy difference between the prolate and oblate shapes becomes smaller and the ground state becomes oblate before reaching the next magic number of 40.

3.6 Splitting of the plasmon resonance

We have estimated the effect of deformation on the splitting of the plasmon resonance using the classical approach explained in Sect. 2.4. Figure 10 shows the calculated plasmon energies for the ground states and the isomers. In the case of a spherical cluster there is only one plasmon energy. Prolate clusters have two high-energy plasmon modes and one low-energy mode, whereas oblate shapes have one high-energy mode and two low-energy modes. In clusters with no axial symmetry, all three energies are generally different. However, in the $N = 18$ cluster the lower energy is degenerate due to the D_3 symmetry.

The splitting of the plasmon resonance is in qualitative agreement with experiment. The results of Borggreen et al.

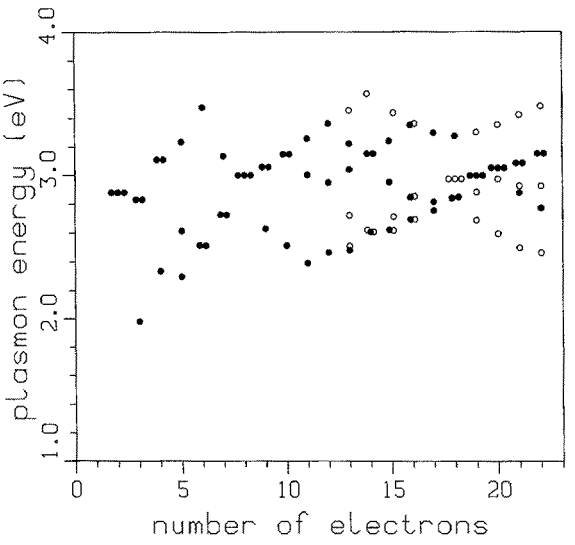

Fig. 10. Plasmon energies for the ground states (*black dots*) and the isomers (*open circles*), calculated in a classical approximation

[10] show that a shape transition occurs from prolate to oblate near $N = 15$, from oblate to spherical at $N = 20$, and back to prolate thereafter.

In Fig. 10 the average plasmon energy for a cluster is around 3 eV. It increases slowly with cluster size, approaching the asymptotic limit of 3.18 eV calculated for an infinite sphere. It is interesting to note that in the ultimate jellium model the plasmon energies for small clusters are closer to the asymptotic limit than in the conventional jellium model [42]. The reason lies in the higher density and smaller size of the clusters in the ultimate jellium model. In small clusters the pressure caused by the surface tension compresses the cluster as seen in Fig. 9.

4 Discussion and conclusions

We have calculated the ground-state and isomeric-state geometries of clusters with 2 to 22 electrons in a jellium model where the positive background density is completely deformable. The model has no input parameters. The cluster geometries were calculated in the local-spin-density approximation with a plane-wave basis. No symmetry restrictions were imposed on the electron density.

The geometries obtained are in qualitative agreement with those found by Frauendorf and Pashkevich [13] using the Strutinsky method, and with those calculated by Hirschmann et al. [15] using a jellium model where the background edge is smoothed out with a Fermi function.

The cluster geometries show large deformations from spherical shape. Breaking of axial and inversion symmetry is usual, and in general the shapes are not ellipsoidal. Some of the clusters seem to be weakly bound "molecules" of magic clusters. All clusters violating inversion symmetry were found to be extremely soft against odd-multipole deformations.

The variation of the total energy per particle is largely determined by the single-electron eigenvalues. The deformation creates a gap at the Fermi level. The gap is almost as large in even nonmagic clusters as in magic clusters. The approximate spin degeneracy of the single-particle levels causes a regular odd-even staggering of the total energy per electron and in the HOMO level. The spin splitting reduces the odd-even staggering by about 30% as compared with a spin-independent formalism. The odd-even staggering and the shell oscillation of the separation energy $E(N) - E(N-1)$ are in fair agreement with the measured monomer dissociation energies of Na clusters [46].

The splitting of the plasmon resonance due to deformations was estimated using a simple classical description, equivalent to the sum-rule approach. The results are in qualitative agreement with experimental results [10] for sodium, whose bulk density is closest to that predicted by the ultimate jellium model.

The ultimate jellium model does not describe any specific metal. Rather, it is a model of the electron gas that yields the optimal cluster shapes from the electrons' point of view. The reason that it can describe some general features of alkali clusters lies in the fact that in those metals the bulk density is close to that of the ultimate jellium model.

The ultimate jellium model can be extended to describe other fermion systems in the local-density approximation. Such systems are nuclear matter, ^{3}He, and electron-hole plasma in semiconductors [34]. The only differences from the present model would be a different local effective potential and a different particle mass.

Recently, Sung et al. [47] have used a pseudopotential method to determine the geometries of small lithium clusters. Their result for the 14-electron cluster is in good agreement with the prolate shape found in the present work. Furthermore, application of quantum molecular dynamics to Na_{14} indicates that even in the liquid state the electronic structure induces a prolate deformation [48].

We wish to thank Sven Bjørnholm, Matthias Brack, Stefan Frauendorf, and Ben Mottelson for several valuable discussions. The software help by Jari Toivanen, Vesa Ruuska, and Tuomo Räisänen is gratefully acknowledged. This work was supported by the Academy of Finland and by the Danish Research Academy.

References

1. Knight, W.D., Clemenger, K., de Heer, W.A., Saunders, W.A., Chou, M.Y., Cohen, M.: Phys. Rev. Lett. **52**, 2141 (1984)
2. Brack, M.: Rev. Mod. Phys. **65**, 677 (1993)
3. Martins, J., Bottet, J.: Surf. Sci. **106**, 261 (1981)
4. Ekardt, W.: Phys. Rev. B **29**, 1558 (1984)
5. Chou, M.Y., Cleland, A., Cohen, M.L.: Solid State Commun. **52**, 645 (1984)
6. Clemenger, K.: Phys. Rev. B**32**, 1359 (1985)
7. de Heer, W.A.: Rev. Mod. Phys. **65**, 611 (1993)
8. Manninen, M., Mansikka-aho, J., Nishioka, H., Takahashi, Y.: Z. Phys. D**31**, 259 (1994)
9. Selby, K., Kresin, V., Masui, J., Vollmer, M., de Heer, W.A., Scheidemann, A., Knight, W.: Phys. Rev. B**43**, 4565 (1991)
10. Borggreen, J., Chowdhury, P., Kabaili, N., Lundsberg-Nielsen, L., Lützenkirchen, K., Nielsen, M.B., Pedersen, J., Rasmussen, H.D.: Phys. Rev. B**48**, 17507 (1993)

11. Ekardt, W., Penzar, Z.: Phys. Rev. B**38**, 4273 (1988); **43**, 1322 (1991)
12. Lauritsch, G., Reinhard, P.-G., Meyer, J., Brack, M.: Phys. Lett. A**160**, 179 (1991)
13. Frauendorf, S., Pashkevich, V.V: Z. Phys. D**26**, S98 (1993); Phys. Rev. B (in print)
14. Rubio, A., Balbás, L.C., Alonso, J.A.: Z. Phys. D**19**, 93 (1991)
15. Hirschmann, Th., Brack, M., Meyer, J.: Ann. Phys. (Leipzig) **3**, 336 (1994); Montag, B., Hirschmann, Th., Meyer, J., Reinhard, P.-G., Brack, M.: Phys. Rev. B (in print)
16. Manninen, M.: Solid State Commun. **59**, 281 (1986)
17. Iñigues, M.P., López, M.J., Alonso, J.A., Soler, J.M.: Z. Phys. D**11**, 163 (1989)
18. Maiti, A., Falicov, L.M.: Phys. Rev. A**44**, 4442 (1991)
19. Uteras-Dias, C.A., Shore, H.B.: Phys. Rev. B**40**, 10345 (1989)
20. Perdew, J.P., Brajczewska, M., Fiolhais, C.: Solid State Commun. **88**, 795 (1993)
21. Vashista, P., Bhattacharyya, P., Singwi, S.K.: Phys. Rev. B**10**, 5108 (1974)
22. Martins, J., Buttet, J., Car. R.: Phys. Rev. B**31**, 1804 (1985)
23. Rao, B.K., Jena, P.: Phys. Rev. B**32**, 2058 (1985)
24. Bonačić-Koutecký, V., Fantucci, P., Koutecký, J.: Chem. Rev. **91**, 1035 (1991)
25. Röthlisberger, U., Andreoni, W.: J. Chem. Phys. **94**, 8129 (1991)
26. Lang, N.D., Kohn, W.: Phys. Rev. B**1**, 4555 (1970)
27. Monnier, R., Perdew, J.P.: Phys. Rev. B**17**, 2595 (1978)
28. Manninen, M., Nieminen, R., Hautojärvi, P., Arponen, J.: Phys. Rev. B**12**, 4012 (1975)
29. Manninen, M., Nieminen, R.M.: J. Phys. F**8**, 2243 (1978)
30. Kohn, W., Sham, L.J.: Phys. Rev. **140**, A1133 (1965)
31. Jones, R.O., Gunnarsson, O.: Rev. Mod. Phys. **27**, 689 (1989)
32. Perdew, J.P., Zunger, A.: Phys. Rev. B**23**, 5048 (1981)
33. Ceperley, D.M., Alder, B.J.: Phys. Rev. Lett. **45**, 566 (1980)
34. Manninen, M.: Phys. Rev. B**34**, 6886 (1986)
35. Chelikowsky, J.R., Troullier, N., Saad, Y.: Phys. Rev. Lett. **72**, 1240 (1994)
36. Brink, D.M., Satchler, G.R.: Angular momentum, 2nd edn., p. 64. Oxford: Clarendon 1968
37. Bohr, A.: Dan. Vidensk Selsk. Mat. Fys. Medd. **26**, 14 (1952)
38. Bohr, A., Mottelson, B.: Nuclear structure, Vol. 2. Reading, MA: Benjamin 1975
39. Yannouleas, C., Broglia, R.A.: Phys. Rev. B**44**, 5793 (1991)
40. Seidl, M., Manninen, M.: Z. Phys. D**33**, 163 (1995)
41. Ekardt, W.: Phys. Rev. B**31**, 6360 (1985)
42. Koskinen, M., Manninen, M., Lipas, P.O.: Phys. Rev. B**49**, 8418 (1994); Z. Phys. D**31**, 125 (1994)
43. Wang, Y., George, T.F., Lindsay, D.M.: J. Chem. Phys. **86**, 3493 (1987)
44. Yoshida, A., Døssing, T., Manninen, M.: J. Chem. Phys. **101**, 3041 (1994)
45. Ahmad, I., Butler, P.A.: Annu. Rev. Nucl. Part. Sci. **43**, 71 (1993)
46. Bréchignac, C., Cahuzac, Ph., Leygnier, J., Pflaum, R., Roux, J. Ph., Weiner, J.: Z. Phys. D**12**, 199 (1989)
47. Sung, M.-W., Kawai, R., Weare, J.H.: Phys. Rev. Lett. **73**, 3552 (1994)
48. Häkkinen, H., Manninen, M.: Phys. Rev. B**52**, 1540 (1995)